Research Article | Vol. 31, No. 4 / 13 Feb 2023 / Optics Express 5832
Optics EXPRESS

Alexandrite lasers with blue-diode-pumping

HUAIFENG XIAO, XUNUO JIANG, AND MICHAEL J. DAMZEN*

Photonics Group, The Blackett Laboratory, Dept. of Physics, Imperial College London, London SW7 2AZ, UK
m.damzen@imperial.ac.uk

Abstract: The availability of high-power and high-brightness blue diode lasers makes them attractive as low-cost pump sources for broadly tunable Alexandrite lasers. In this paper we investigate the performance of an Alexandrite laser pumped by a high-power fiber-delivered blue diode module. Output power 1.84 W is achieved, the highest power from blue diode pumped Alexandrite to date. Excellent pump absorption is demonstrated of scrambled pump polarization on both *a*-axis and *b*-axis of Alexandrite crystal. Wavelength tuning and dual wavelength operation is produced using the self-birefringent filtering of the Brewster-cut Alexandrite crystal. An analysis is made of laser efficiency and mode formation including the creation of higher-order Laguerre-Gaussian vortex modes (LG_{01} and LG_{02}). Performance is compared to red diode pumping and prospects for further optimization and power-scaling are discussed.

1. Introduction

Alexandrite is a broadly tunable solid-state laser in the useful near-IR wavelength region (~700 - 800 nm). It has very favourable thermo-mechanical properties, including high thermal conductivity and mechanical strength that allow for high power scalability [1]. Its long upper-state lifetime (~260 μs at room temperature) is suitable for high energy Q-switched operation [2], and with harmonic conversion direct production of tunable UV and deep UV can be achieved. To address its many potential applications including in medical therapeutics, remote sensing, and quantum technologies, it is important to realise high-performance operation of Alexandrite in low cost and compact format with potential for power scaling. The main recent development in diode-pumped Alexandrite has been using red diode pumping, but the maturity of high power blue GaN-based laser diodes with higher-brightness than red diodes and low cost ($/W) makes them of interest for pumping Alexandrite. The aim of this paper is to make an investigation of high-power blue diode pumping of Alexandrite for which we use a fiber-coupled blue pump module, for the first time to our knowledge.

The energy level system of Alexandrite is shown in Fig. 1(a). Four-level laser emission occurs from the $^4T_2 \rightarrow {}^4A_2$ vibronic transition which at room temperature has a broad fluorescence spectrum with a useful lasing wavelength band extending from ~ 720–820 nm [3]. At elevated temperatures the lasing wavelength has been extended as far as 858 nm [4]. With high inversion to overcome ground-state absorption loss, lasing wavelength as short as 701 nm has been produced [1]. There is also a long-lived three-level transition $^2E \rightarrow {}^4A_2$ with a pair of narrow lines, the so-called R-lines, at 680.4 nm and 678.9 nm. Alexandrite is a biaxial crystal with strong birefringence along three orthogonal principal axes with distinct refractive indices and absorption/emission cross-sections. The laser emission is strongly polarized parallel to the crystal *b*-axis which possesses the largest emission cross-section. Figure 1(b) shows the three distinct absorption spectra for polarisation parallel to the three crystal axes. It is noted that there is a pronounced difference in spectral shape between the three axes, however in all cases there are two main peaks: in the yellow-red (centred at 590 nm, for *b*-axis) corresponding to the $^4A_2 \rightarrow$

#482582 https://doi.org/10.1364/OE.482582
Journal © 2023 Received 8 Dec 2022; revised 14 Jan 2023; accepted 14 Jan 2023; published 2 Feb 2023

Optics EXPRESS

$^4T_2$ band and in the blue (centred at 420 nm) corresponding to the $^4A_2 \rightarrow {}^4T_1$ band. The broad spread of these two main vibronic bands of Alexandrite provides absorption covering the entire visible spectrum. It is another of Alexandrite's attractive features allowing efficient broadband lamp-pumping [1], pumping by visible semiconductor (diode) lasers [2,3,5], and other visible sources including Kr-ion [6], dye [5], frequency-doubled Nd:YAG and Nd:YVO_4 laser [6,7] and even using LED pumping [8].

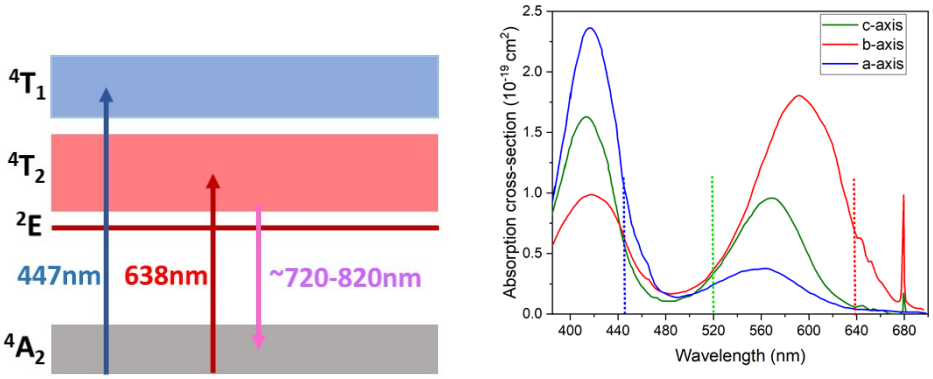

(a) (b)

Fig. 1. a) Energy level structure; and b) absorption spectra of Alexandrite (after [1]), dashed lines indicate key diode wavelengths: red 638 nm; green 520 nm; blue 445 nm.

Diode-pumping provides an order of magnitude increase in efficiency to lamp pumping and has driven a renewed research and application-focused development in Alexandrite lasers. Compared to other non-diode laser pump sources (e.g., frequency-doubled Nd:YAG lasers), diode lasers offer significantly better overall electrical-to-optical efficiency with lower service requirements, more compact format, and high-power scaling at very low pump cost. To date, almost all diode-pumping has been with red semiconductor lasers near 638 nm although in-band pumping directly to the narrow ^2E line at 680 nm has been performed [9]. The 638 nm wavelength is the most developed red diode for display applications including the development of high-power (tens – 100 Watt) modules with multiplexed diode-bars or single-emitters coupled into fiber-delivered units. Using red diode pumping significant advances in diode-pumped Alexandrite lasers has been achieved in recent years, including output power > 26 W [10], high-energy Q-switched pulsing to > 3 mJ [2], broad tunability > 100 nm [3], harmonic conversion to UV [2], and systems developed for space-borne Lidar [11].

Given the broad absorption spectrum of Alexandrite other diode wavelengths can be considered. Green diodes near 520 nm are possible to use, but their development has been slower than blue diodes and delivering relatively moderate powers and lower efficiency. Green diodes also operate in the weakest absorption region of Alexandrite making it harder to achieve spatial overlap of the pump with the laser mode over a long absorption depth in the laser crystal.

Blue diode lasers near 445 nm on the other hand have developed with spectacular success outperforming other visible diode lasers including red diodes in terms of power, brightness, and cost ($/W). Blue single-emitter diodes now provide the highest visible power 6 W compared to ~2 W for red (and ~1 W for green diodes). They operate with ~ 40% wall-plug efficiency comparable to red diodes and considerably exceeding green diodes. The smaller blue emitter size (lower M^2 or beam parameter product) and higher power make them much brighter sources (watts/area/steradian) which is an important property required for high power end-pumping of solid-state lasers. Both blue and red diodes are power scaled by multiplexing single emitters

Optics EXPRESS

or diode bars including fiber-coupling. Blue diode-bars and multiplexed single emitters at the multi-100 W and multi-kW power levels now out-perform red diodes driven by industrial material processing of metals, particularly copper for battery production where the high blue absorption is a major enhancement for processing speed [12].

It is the purpose of this paper to investigate the use of high-power blue diode pumping of Alexandrite based on the availability of high-power, high brightness and low-cost blue diode modules. Prior work on blue-diode pumping of Alexandrite has been done by Fibrich et al. [13,14] using a 3.5 W single-emitter diode laser, principally looking at cryogenic cooling of Alexandrite, spectroscopy of Alexandrite with temperature, and laser operation in a microchip structure with laser cavity formed by the coated crystal faces. In this prior work, demonstration was made of three-level continuous-wave operation of Alexandrite at 680 nm at low cryogenic crystal temperatures and vibronic four-level operation at 750 nm at higher temperatures producing over 0.5W pumped by a single emitter blue diode at 445 nm.

In this paper, we present investigations and results of a Brewster-cut Alexandrite crystal pumped by a high-power fiber-delivered blue diode module operating in the range 444–448 nm with > 10W power. We achieve 1.84 W power, the highest power to date from blue diode pumped Alexandrite. The blue pump absorption uses the $^4A_2 \rightarrow {}^4T_1$ band where the spectral response gives highest absorption at the crystal *a*-axis. However, we demonstrate that there is also excellent absorption on the *b*-axis to allow near to 100% absorption of unpolarized light as occurs in high-power fiber-delivered pump modules. We perform a full spatial and mode formation investigation and analysis of the blue-diode pumped Alexandrite laser, including the creation of high-order Laguerre-Gaussian LG_{01} and LG_{02} (vortex) modes. Wavelength tuning and dual wavelength operation is demonstrated and analysed as function of crystal temperature and absorbed pump power heating using the birefringent filter effect of the Brewster-cut crystal. A consideration is made of the efficiency factors and impact of the high quantum defect heating that occurs by blue pumping compared to red pumping, and prospects discussed for further optimization and power-scaling.

2. Experimental blue-diode-pumped Alexandrite laser system and results

2.1. Experimental laser system

Figure 2 shows the experimental laser system used for this investigation. The blue-diode pump laser was a fiber-delivered diode module with compact package dimensions $50 \times 42 \times 18$ mm. The module was mounted on a water-cooled heat-sink for temperature control. The diode delivery fiber had a core diameter of 105 µm and numerical aperture NA = 0.22. The output pump power was greater than 10W. Its wavelength varied from 444 nm to 448 nm as its power was increased from low to maximum. The optical output from the delivery fiber was collimated with a lens (f_c) with focal length 35 mm and then focused with a second pump lens (f_p) into the Alexandrite laser crystal. The spatial quality of the focused pump beam was measured to have a beam propagation factor $M^2 \approx 75$. The polarisation of the pump beam was partially scrambled with a 60:40 power split between its major and minor polarisation axes. A half-wave plate (HWP) was used to orientate the polarisation for maximised absorption in the Alexandrite crystal.

The Alexandrite laser was formed by a Brewster-cut Alexandrite laser crystal in a compact linear resonator with a dichroic plane back mirror (BM) with high reflectivity at lasing waveband (700–820 nm) and high transmission at the pump wavelength (reflection loss <0.5% at 447 nm), and a partially-reflecting plane front mirror acting as output coupler (OC). The cavity length was approximately 16 mm. The Brewster-cut Alexandrite crystal was chosen in preference to a plane-cut crystal since the stock we had were AR-coating for red-diode pumping and this coating was too reflective (~40%) at the blue pump wavelength. The Brewster-cut Alexandrite crystal had 0.24 at.% Chromium doping and was in the form of a slab with 4×4 mm cross-section and 8 mm length. The crystal was c-cut, with the *b*-axis in the direction of the horizontal plane containing

Optics EXPRESS

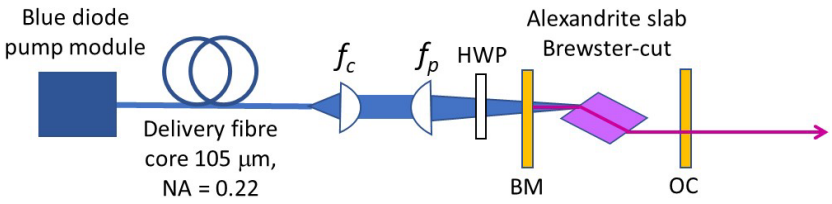

Fig. 2. Experimental blue-diode-pumped Alexandrite laser system.

the Brewster-angle and the *a*-axis in the vertical direction. It was the same crystal (crystal 2) used in one of our previous investigations [15] using red-diode pumping of Alexandrite, allowing us to make some direct comparison between blue-diode and red-diode pumping laser performance. The crystal was mounted and clamped on top of a water-cooled copper holder for temperature control with heat conduction from the base of the crystal.

The refractive index of Alexandrite at pump wavelength ($n \approx 1.76$) is sufficiently the same as at the lasing wavelength ($n = 1.74$) for the Brewster angle to be low Fresnel reflection loss at both pump and laser wavelength for *p*-polarized light. Since the polarisation of the fiber-delivered pump was partially scrambled there was a Fresnel reflection loss ~ 25% for the s-polarized pump component at the crystal Brewster-face, resulting in a net (measured) reflection loss ~ 12% of the total incident pump power. Accounting for the reflection loss and measured pump transmission through the crystal the effective absorption coefficient for the blue pump was calculated to be ~0.7 mm^{-1} and overall, the absorbed pump power was ~87% of the incident pump power.

2.2. Laser output power

Figure 3 shows the Alexandrite laser output power versus absorbed blue pump power for a crystal holder temperature $T_{xtal} = 10 \circ C$, and output coupler with reflectivity $R_{OC} = 99\%$. Two pump focal length lenses were investigated: $f_p = 75$ mm and $f_p = 50$ mm producing focal pump diameter at the crystal of 310 µm and 230 µm, respectively. For the 75 mm lens, an output power of 1.25 W was produced for 9.6 W of absorbed pump power. The threshold pump power was ~3.7 W, and a linear fit to the power data gives a laser slope efficiency of 21%. For the 50 mm pump lens, an output power of 1.84 W was produced, the highest power to date for a blue-diode-pumped Alexandrite laser. The threshold pump power was ~2.5 W, with a laser slope efficiency of 26%.

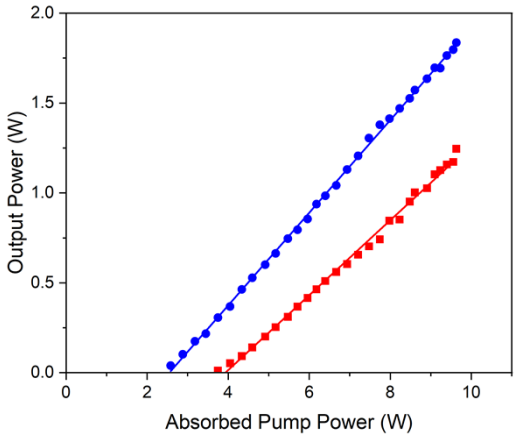

Fig. 3. Laser power versus absorbed pump power with pump lens $f = 75$ mm (red data) and 50 mm (blue data) ($T_{xtal} = 10 \circ C$; $R_{OC} = 99\%$).

Optics EXPRESS

An investigation was made of output laser power as a function of Alexandrite crystal temperature. Figure 4 shows laser output power as a function of crystal holder temperature varied from 10°C to 60°C at fixed absorbed pump power of 8.9 W and f_p = 75 mm pump lens. Laser power is notably highest at lower temperatures and decreases at higher temperatures. It is noted that this trend is opposite to normal experience of Alexandrite laser operation when performance usually observed to increase somewhat with higher temperature. The exact reason is unknown but may be a feature of Brewster-cut crystal and the detailed pump-induced internal heating of the crystal that will be discussed further in Section 2.4. The pronounced temperature dependence of laser power was the reason the laser crystal was operated at 10°C in the results shown in Fig. 3.

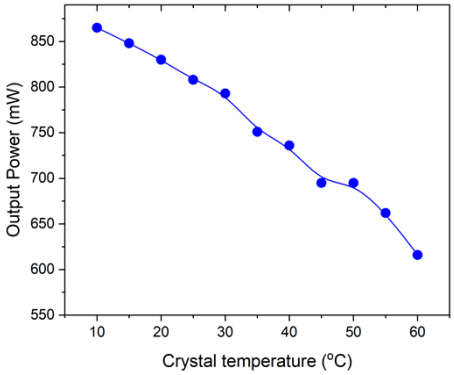

Fig. 4. Laser output power versus crystal temperature (f_p = 75 mm, P_p = 8.9 W, R_{OC} = 99%).

2.3. Spatial quality

An investigation of spatial beam quality of the laser was performed using a beam profiling camera system. Figure 5 shows the spatial mode size (diameter) and the corresponding M^2 beam propagation factor both measured using the second moment method and for the horizontal (x) and vertical (y) directions, for both pump lens cases f_p = 75 mm (Fig. 5(a)) and f_p = 50 mm (Fig. 5(b)). The spatial size is slightly elliptical with smaller horizontal than vertical size. This is expected due to the Brewster-cut of the crystal that reshapes the pump size in the horizontal and introduces astigmatism in the laser mode. The spatial quality is near diffraction-limited $M^2 \approx 1$ near threshold, with operation in fundamental mode. As fundamental mode diameter underfills the gain region (d_p = 310 μm for f_p = 75 mm; d_p = 230 μm for f_p = 50 mm), higher-order mode formation occurs increasing M^2 up to ≈2.5 – 3.0 at maximum pump power.

A simple cavity analysis was made to predict laser mode size and understand spatial quality. In our modelling, the pump-induced thermal lens produced at the input face of the Alexandrite crystal with focal length f is taken together with the plane back mirror as equivalent to a back cavity mirror with radius of curvature $R_1 = f$. The fundamental (Gaussian) mode diameter size at the back mirror (the gain medium location) is given by laser mode theory

$$d_1 = 2w_1 = 2\left(\frac{\lambda L}{\pi}\right)^{1/2}\left(\frac{g_2}{g_1(1-g_1g_2)}\right)^{1/4} \approx 2\left(\frac{\lambda}{\pi}\right)^{\frac{1}{2}}\left(\frac{L}{D}\right)^{\frac{1}{4}} \tag{1}$$

where λ is laser wavelength; L is the cavity length accounting for refractive index of Alexandrite; $g_1 = 1 - L/R_1 = 1 - L/f$, $g_2 = 1 - L/R_2 = 1$ are the cavity g-parameters. The latter solution in Eq. (1), is valid for compact cavity $L \ll f$, as in our case, and where pump-induced lens dioptric power $D = 1/f$. For the vertical direction in Brewster-cut crystal the effective cavity

Optics EXPRESS

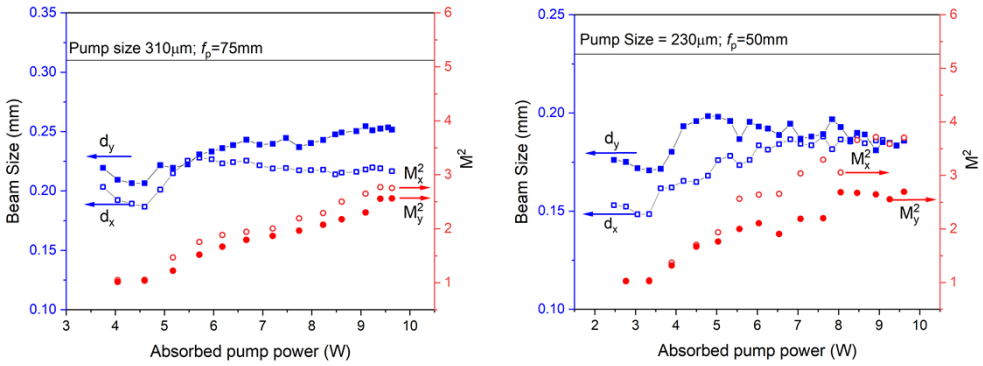

Fig. 5. Laser beam size (d_x; d_y: blue open; closed squares) and M^2 (M_x^2; M_y^2: red open; closed circles) vs absorbed pump power, for pump lenses (a) f_p = 75 mm; (b) f_p = 50 mm.

length $L = L_y = l_{air} + l_G/n \approx 12$ mm, crystal length l_G = 8 mm, air length l_{air} = 8 mm and we take λ = 765 nm in experiments. Table 1 shows a summary of key results of pump size, pump threshold, vertical laser mode diameter and beam quality, and dioptric lensing power for the f_p = 50 mm and 75 mm pump lenses.

Table 1. Summary of laser parameters for the two pump lens cases

	f_p = 50 mm	f_p = 75 mm
Pump diameter $d_p(\mu m)$	230	310
Pump threshold power $P_p^{th}(W)$	2.5	4.0
Laser mode diameter $d_{1y}(\mu m)$	175	210
Beam quality at threshold M^2	1.0	1.0
Dioptric lens power per unit pump power $D_{0y}(m^{-1}W^{-1})$	2.5	1.4

Comparing the two pump lenses, the ratio of pump focal areas, and hence reciprocal of focal pump intensities, is $(310\mu m/230\mu m)^2 = 1.82$, the corresponding ratio of threshold pump powers ~3.8W/2.5W = 1.52, and the ratio of lensing strength D_{0y} per watt of pumping ~2.5/1.4 = 1.79. All these ratios are comparable as expected, although it is noted that the pump beam Rayleigh length in Alexandrite crystal for the f_p = 50 mm lens is approximately equal to the pump absorption depth $1/\alpha_p \sim$ 1.4mm and its effective pump diameter over the region of pump inversion is somewhat larger than its focal diameter.

When going up to maximum pumping the thermal lensing power D increases and the fundamental mode size would be predicted to decrease by Eq. (1). The fundamental mode increasingly under-fills the pump volume allowing the onset of higher-order modes with increasing M^2 producing multimode beam diameter given by $d_M = \sqrt{M^2}\, d_1$ where d_1 is the fundamental mode diameter. It is noted from the mode diameter results of Fig. 5, that even in multimode operation there is significant underfilling of the gain region, and the impact of this will be analysed further in discussion section of this paper.

2.4. *Spectral behavior and its temperature dependence*

Figure 6 shows the peak emission laser wavelength for the f_p = 75 mm pump lens. Figure 6(a) shows laser wavelength as a function of pump power at fixed crystal holder temperature of 15°C.

Optics EXPRESS

The laser operates on a single narrow spectral band, but over a narrow pumping range near 6W operates on dual wavelength with spectral separation ~13 nm. The individual spectral lines tune to shorter wavelength with pump power at a rate of approximately -0.50 nm/W. Figure 6(b) shows the wavelength tuning produced by varying temperature of the laser crystal holder at fixed absorbed pump power of 8.9 W. The laser wavelength shifts with increasing temperature at a rate -0.07 nm/°C. Between 25°C – 30°C the laser runs dual wavelength, again with 13 nm separation.

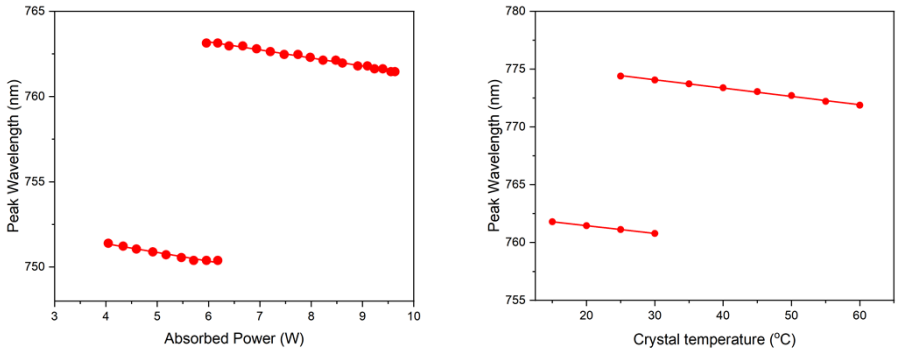

Fig. 6. Lasing wavelength as a function of the a) absorbed pump power, and b) crystal holder temperature.

This spectral tuning with crystal temperature was the same as seen in our previous work with this crystal with red diode pumping with tuning rate -0.07 nm/°C [15]. The tuning behavior can be explained by a birefringent filter effect produced by the birefringent Alexandrite crystal combined with its Brewster-cut faces providing a reflection loss mechanism for s-component of polarisation. In reference 15, we show for this Brewster-cut crystal that there is a vertical misalignment of the c-axis ~ 4° which would be a reason for the birefringence to occur when crystal is at Brewster angle. The wavelength shift with temperature is due to the variation in crystal refractive index birefringence $\Delta n(T)$ between b-axis and a-axis [15]. The dual wavelength operation with 13 nm separation is the free-spectral range ($\Delta\lambda_{FSR} = \lambda_0^2/\Delta nL$) of the laser crystal with mean wavelength $\lambda_0 \sim 760$ nm and crystal length $L \approx 8$ mm.

The pump-power dependent wavelength shift can be identified as due to the internal crystal heating produced by the absorbed pump. By comparing the rate of wavelength shift with pump power -0.50 nm/W with the shift due to direct crystal holder temperature change -0.07 nm/°C, it is deduced that the effective internal crystal temperature change with respect to absorbed pump power as seen by the laser mode is approximately 7 °C/W. At maximum pumping of 9.6 W this corresponds to an internal crystal temperature rise ~ 67°C. With crystal holder at 15°C, this is an effective absolute temperature ~82°C seen by the laser mode, assuming minimal thermal resistance between the copper holder and the crystal contact.

A theoretical estimate can be made of the expected temperature rise ΔT at the centre of end-pumped Alexandrite crystal ($r = 0$) relative to its conduction-cooled edge (at $r = r_0$) [16]

$$\Delta T = T(0,z) - T(r_0,z) = \frac{\eta_h \alpha_p P_p(z)}{4\pi\kappa}\left[ln\left(\frac{r_0^2}{w_p^2}\right) + 1\right] \tag{2}$$

where the formula applies to approximating crystal as a rod (radius $r_0 = 2$ mm) with top-hat pump beam (radius $w_p = 0.15$ mm) and taking pump absorption coefficient $\alpha_p = 0.7\ mm^{-1}$, thermal conductivity $\kappa = 23\ \mathrm{Wm^{-1}K^{-1}}$ and heating factor $\eta_h = \eta_D = 1 - \lambda_p/\lambda_L = 0.41$ equal to quantum defect η_D for pump wavelength $\lambda_p = 447\ nm$ and lasing wavelength $\lambda_L \sim 760\ nm$. According

Optics EXPRESS

to Eq. (2), the increase in temperature per Watt of incident pump power P_p is predicted to be $d(\Delta T)/dP_p = 6$ ∘C/W. This value is consistent with 7 °C/W from the previous temperature analysis of experimentally observed birefringence-induced wavelength tuning of the crystal.

As well as the slow wavelength tuning to shorter wavelength and occurrence of dual wavelength operation with 13 nm separation seen in both Fig. 6(a) and 6(b), there is an overall trend to lasing at longer wavelength with increasing temperature, whether due to us directly increasing temperature of crystal holder or by pump induced heating. This can be seen in Fig. 6(a) with wavelength jumping from ∼ 750 nm to 763 nm and in Fig. 6(b) with wavelength jump from 761 nm to 774 nm. The wavelength shift with temperature is well documented for Alexandrite but with discrete jumps in our experiment due to the birefringent filtering by the Brewster-cut crystal. It is also noted that more general wavelength tuning can be achieved by tilting the Brewster crystal in the vertical or horizontal direction as detailed in our prior work [15].

2.5. Spatial mode formation

Figure 7 shows examples of spatial mode formation in the laser cavity with $f_p = 75$ mm pump lens at different pump powers for the two output coupling mirrors $R_{OC} = 99\%$ and $R_{OC} = 99.5\%$. For the case of $R_{OC} = 99\%$, Fig. a-c show that with increasing pump power the laser spatial mode goes from fundamental Gaussian mode to higher order mode in a mode superposition. In the case of $R_{OC} = 99.5\%$, with increasing pump power the laser spatial mode goes from fundamental Gaussian mode with $M^2 \approx 1.0$ (Fig. 7(d)), to a pure Laguerre-Gaussian LG_{01} vortex mode (Fig. 7(e)) with central dark singularity with topological charge 1 and measured $M^2 \approx 2.01$ (theoretical LG_{01} vortex mode $M^2 = 2.0$). At higher power (Fig. 7(f)) we obtain a spatial form we associate with a LG_{02} mode with topological charge 2, however it has a displaced pair of singularities that can be associated with the cavity astigmatism arising from the Brewster-cut of the crystal. The exact reason for the difference in the spatial with the two output couplers is not well understood but it can be conjectured that the purer mode formation with $R_{OC} = 99.5\%$ must be associated with the higher intracavity flux affecting mode competition. The pump distribution is near-Gaussian, and this will give rise to a thermally-induced lens with spherical aberration [17] and there is known to be a pronounced difference in lensing strength that has been observed in Alexandrite between non-lasing and lasing [18]. Formation of structured modes with defined singularities has interesting potential applications for optical trapping and levitation [19].

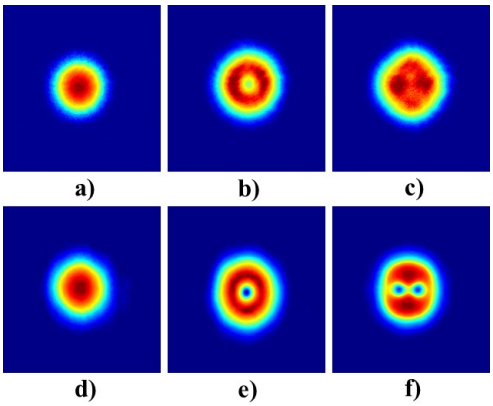

Fig. 7. Spatial mode patterns for $R_{OC} = 99\%$ at pump power a) 4.5 W, b) 6.5 W, and c) 8.5 W; and in cavity with $R_{OC} = 99.5\%$ at pump power d) 3.7W, e) 5.5 W, and f) 8.0 W.

Optics EXPRESS

3. Discussion

The blue-diode-pumped Alexandrite laser has operated with good performance. A key parameter for laser performance is the laser slope efficiency, which was 26% for the case of f_p = 50 mm pump lens and R_{OC} = 99% output coupler. To understand the laser efficiency, a calculation can be performed of the various laser efficiency factors. For the blue-pump wavelength λ_p = 447 nm, the Stokes efficiency $\eta_{st} = \lambda_p/\lambda_L = 447/760 = 59\%$ is the ratio of laser to pump photon energy. We measured threshold pump powers with different output couplers ($T_{OC} = 1 - R_{OC} = 0.25\%,\ 0.5\%,\ 1.0\%$) and performed a Findlay-Clay analysis [20] to deduce an intracavity roundtrip loss $L_C \approx 0.35\%$. For output mirror R_{OC} = 99% (T_{OC} = 1.0%) we can define a laser output coupling efficiency $\eta_{OC} = T_{OC}/(T_{OC} + L_C) = 74\%$. The spatial overlap between laser mode diameter $d_L \approx 180$ μm and pump diameter d_p = 230 μm (produced by f_p = 50 mm pump lens), gives a beam area overlap efficiency $\eta_B = (d_L/d_p)^2 = 61\%$. Combining these factors gives a predicted laser slope efficiency $\eta_S = \eta_{st}\eta_{OC}\eta_B = 26.6\%$. This is consistent with our measured slope efficiency 26%. It highlights that efficiency could be significantly improved with better optimization of output coupling mirror and better beam area overlap using optimized focal pump size and cavity design. This prospect is evidenced by prior blue-pumping at 445 nm of a "microchip" Alexandrite laser with cavity mirrors formed by the surface coatings on the 2.5 mm long crystal, with $R_{OC} \sim 120$ 98%, where a slope efficiency of 39% was achieved [14]. The output coupling efficiency in the simple monolithic cavity of Ref. [14] would be near unity and with the small pump diameter $d_p \sim 120$ μm used should have high beam overlap efficiency.

It is interesting to compare blue-diode pumping performance with red-diode pumping. For this same Brewster-cut Alexandrite crystal used in this study was also used in a laser system with fiber-delivered red-diode pumping at 637 nm [15]. A slope efficiency up to 49% was achieved when operating crystal at $10 \circ C$ in a compact cavity [15]. The red-pump slope efficiency is intrinsically higher due to the better Stokes efficiency $\eta_{st} = \lambda_p/\lambda_L = 637/760 = 84\%$ (1.42 times higher than blue pump) but additionally a smaller red pump diameter d_p = 150 μm was used in Ref. [15] then in our blue-pumped laser so a better beam mode area overlap efficiency is expected.

Another factor to consider for blue diode pumping is the higher quantum defect heating $\eta_D = 1 - \lambda_p/\lambda_L = 41\%$, compared to η_D = 16% for the red pump. This should lead to a factor of 2.6 times higher thermally-induced lensing strength for the blue pump, creating greater challenge for power scaling and operation in high spatial quality mode. On the positive side, the Alexandrite crystal in our system was demonstrated to be able to be strongly absorb both *a* and *b* polarization components of the blue pump module. We achieved ~ 87% absorption of almost unpolarized incident pump light, the main loss (~12%) coming from the s-polarisation reflection at the Brewster crystal face. With use of suitably coated plane crystal faces, we would expect ~ 99% pump absorption. This is highly beneficial for maximum absorption efficiency of unpolarized high power pump modules that often use polarization-combined multiple diode emitters or due to the polarization scrambling caused by fiber-delivery. Considering the absorption spectra in Fig. 1(b), all three polarization states see good absorption in the blue. As seen in Fig. 1(b), at 445 nm wavelength, the *a*-axis absorption is significantly higher and the *b*-axis absorption similar to the absorption with red pumping at 638 nm on the *b*-axis. For the case of the red pumping, only the *b*-axis polarization component is well absorbed in Alexandrite, the other polarization component has order of magnitude lower absorption cross-section. A double-pass scheme has been devised to absorb both pump polarization states [21] for the red-pumping but is more cumbersome to implement than a simple single-end-pumping scheme.

We can further confirm in this study that there was no evidence of any transient blue-induced crystal degradation in Alexandrite that has been observed to occur in blue-diode pumping of Ti:sapphire laser crystals [22].

Optics EXPRESS

4. Conclusions

This paper presents an investigation of an Alexandrite laser with high-power fiber-delivered blue diode-pumping at ~447 nm. A laser output power of 1.84 W is achieved, the highest power to date for a blue-diode-pumped Alexandrite laser. Excellent absorption efficiency is demonstrated on both the crystal *a*-axis and *b*-axis, with a net effective absorption coefficient ~ 0.7 mm^{-1} which is higher than with red pumping at 638 nm on the *b*-axis. An absorption ~ 87% of almost unpolarized incident pump light was measured with inefficiency almost entirely due to the reflection loss at the crystal Brewster face. This shows the potential for near 100% absorption of even an unpolarized blue pump module near 445 nm with suitably coated plane crystal faces.

The laser slope efficiency was 26% which is good but an analysis of intracavity loss and spatial mode size showed this could be improved considerably by optimization of laser output coupling mirror and mode area overlap with pump volume using optimized pump size and better cavity design. Spatial beam investigation was made of second moment mode size, beam quality M^2, and mode structure. The ability to generate vortex modes under certain cavity configuration was shown.

An investigation of output wavelength showed narrow line lasing that tuned with both laser crystal temperature and absorbed pump power. The rise in temperature of the laser crystal due to pump absorption is correlated to the laser wavelength tuning with temperature variation of crystal holder. Dual wavelength operation was achieved over narrow temperature or pump power ranges. Both the wavelength tuning behavior and dual wavelength operation is fully quantifiable by a self-birefringent filtering effect in the Brewster-cut Alexandrite crystal.

In comparison to red diode pumping, the blue pumping is less efficient with respect to absorbed pump power, as expected by the lower Stokes efficiency of the blue pump. A key challenge for power scaling Alexandrite will be the high quantum defect heating in the blue compared to red diodes, meaning blue pumps are unlikely to displace red diode pumping at high power levels. However, superior pump absorption is possible with blue pumping, especially for unpolarized light as commonly occurring in high-power fiber delivered pump modules. This allows superior efficiency with respect to incident pump power and overall higher electrical (wall-plug) efficiency of blue diodes compared to red diodes. The recent availability of very high power and higher brightness blue fiber-delivered pump modules (even to kW powers) means blue-pumping of Alexandrite is a viable pump option to consider and lower cost ($/W) of blue pumping would also be a commercial consideration for product development.

Funding. European Space Agency (4000115840/15/NL/PA/zk).

Acknowledgments. The authors thank Dr. A. Minassian for technical advice, and Martin Kehoe and Simon Johnson for manufacture of mechanical workshop parts.

Disclosures. The authors declare no conflicts of interest.

Data availability. Data underlying the results presented in this paper are not publicly available at this time but may be obtained from the authors upon reasonable request.

References

1. J. Walling, O. Peterson, H Jenssen, R. Morris, and E. O'Dell, "Tunable Alexandrite lasers," IEEE J. Quantum Electron. **16**(12), 1302–1315 (1980).
2. G. Thomas, A. Minassian, X. Sheng, and M.J. Damzen, "Diode-pumped alexandrite lasers in Q-switched and cavity-dumped Q-switched operation," Opt. Express **24**(24), 27212–27224 (2016).
3. W.R. Kerridge-Johns and M.J. Damzen, "Temperature effects in tunable cw Alexandrite lasers under diode end-pumping," Opt. Express **26**(6), 7771–7785 (2018).
4. J.W. Kuper, T. Chin, and H.E. Aschoff, "Extended Tuning Range of Alexandrite at Elevated Temperatures," in *Advanced Solid State Lasers, vol. 6 of OSA Proceedings Series* (Optical Society of America, 1990) p. CL3.
5. R. Scheps, J.F. Myers, T.R. Glesne, and H.B. Serreze, "Monochromatic end-pumped operation of an Alexandrite laser," Opt. Commun. **97**(5-6), 363–366 (1993).
6. S.T. Lai and M.L. Shand, "High efficiency cw laser-pumped tunable alexandrite laser," J. Appl. Phys. **54**(10), 5642–5644 (1983).

Optics EXPRESS

7. S. Ghambari, R. Akbari, and A. Major, "Femtosecond Kerr-lens mode-locked Alexandrite laser," Opt. Express **24**(13), 14836–14840 (2016).
8. P. Pichon, A. Barbet, J-P. Blanchot, F. Druon, F. Balembois, and P. Georges, "LED-pumped alexandrite laser oscillator and amplifier," Opt. Lett. **42**(20), 4191–4194 (2017).
9. E. Beyatli, I Baali, B. Sumpf, G. Erbert, A. Leitenstorfer, A. Sennaroglu, and U. Demirbas, "Tapered diode-pumped continuous-wave alexandrite laser," J. Opt. Soc. Am. B **30**(12), 3184–3192 (2013).
10. A. Teppitaksak, A. Minassian, G.M. Thomas, and M.J. Damzen, "High-efficiency >26W diode end-pumped Alexandrite laser," Opt. Express **22**(13), 27212–27224 (2014).
11. A. Munk, B. Jungbluth, M. Strotkamp, H.-D Hoffmann, R. Poprawe, J. Hoffner, and F.-J. Lubken, "Diode-pumped alexandrite ring laser in single-longitudinal mode operation for atmospheric lidar measurements," Opt. Express **26**(12), 14928–14935 (2018).
12. M. Baumann, A. Black, J. Malchus, R.V. Chacko, and U. Strauss, "1000 W blue fibre-coupled diode-laser emitting at 450 nm," Proc. SPIE **10900**, 1090005 (2019).
13. M. Fibrich, J. Sulc, D. Vyhlidal, H. Jelinkova, and M. Cech, "Alexandrite spectroscopic and laser characteristic investigated within a 78-400 K temperature range," Laser Phys. **27**(11), 115801 (2017).
14. M. Fibrich, J. Sulc, and H. Jelinkova, "Alexandrite microchip lasers," Opt. Express **26**, 14928–14935 (2018).
15. G. Tawy and M.J. Damzen, "Tunable, dual wavelength and self-Q-switched Alexandrite laser using crystal birefringence control," Opt. Express **27**(13), 17507–17520 (2019).
16. S. Chenais, F. Balembois, F. Druon, G. Lucas-Leclin, and P. Georges, "Thermal Lensing in diode-pumped Ytterbium lasers – Part I: Theoretical analysis and wavefront measurements," IEEE J. Quantum Electron. **40**(9), 1217–1234 (2004).
17. W. A. Clarkson, "Thermal effects and their mitigation in end-pumped soldi-state lasers," J. Phys. D: Appl. Phys. **34**(16), 2381–2395 (2001).
18. G. Tawy and M.J. Damzen, "Pump-induced lensing effects in diode-pumped Alexandrite lasers," Opt. Express **27**(24), 35865–35883 (2019).
19. M.J. Damzen, W.R. Kerridge-Johns, and J.W.T. Geberbauer, "Vortex mode transformation interferometry," J. Opt. **22**(1), 015604 (2020).
20. D. Findlay and R. A. Clay, "Measurement of internal losses in 4-level lasers," Phys. Lett. **20**(3), 277–278 (1966).
21. E.A. Arbabzadah and M.J. Damzen, "Fibre-coupled red diode-pumped Alexandrite TEM_{00} laser with single and double-pass end-pumping," Laser Phys. Lett. **13**(6), 065002 (2016).
22. P. W. Roth, A.J. Maclean, D. Burns, and A. J. Kemp, "Directly diode-laser-pumped Ti:sapphire laser," Opt. Lett. **34**(21), 3334–3336 (2009).